Supporting online material

Molecular Basis of mRNA Recognition by the Specific Bacterial Repressing Clamp RsmA/CsrA

Mario Schubert, Karine Lapouge, Olivier Duss, Florian C. Oberstrass, Ilian Jelesarov, Dieter Haas, Frédéric H.-T. Allain

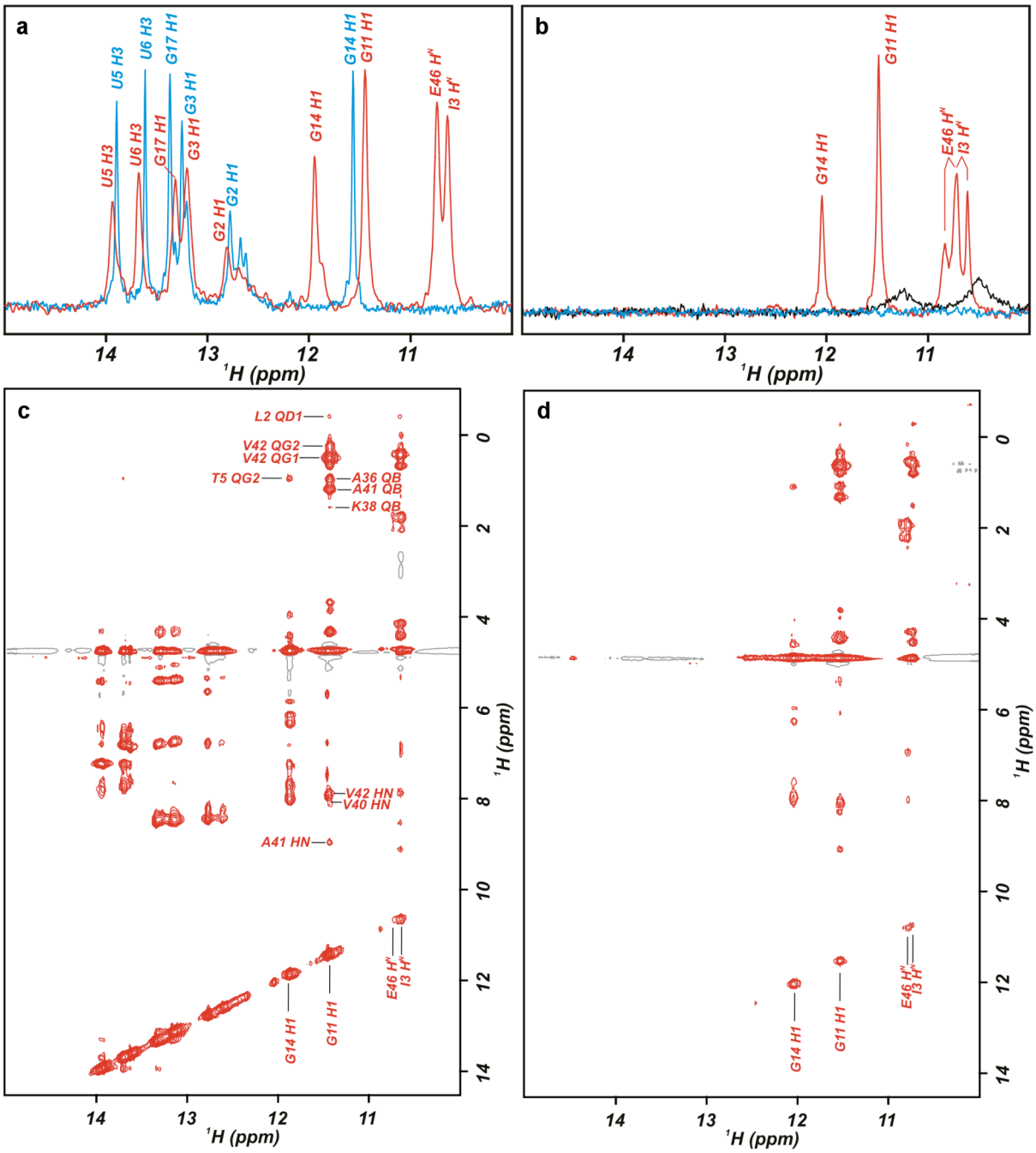

Figure S1: Comparison of NMR spectra between the *hcnA* 20-mer and *hcnA* 12-mer RNA free and in complex with ^{15}N labeled RsmE. (a) Overlay of the imino region in ^{1}H spectra of the *hcnA* 20-mer free (in cyan) and in complex (red) at 40°C. **(b)** Overlay of the imino region in ^{1}H spectra of the *hcnA* 12-mer free (in cyan at 30°C, in black at 3°C) and in complex (red) at 30°C. No ^{15}N decoupling was employed resulting in a splitting of the H^N signals of the protein. **(c)** Imino region of a 2D NOESY spectrum in H_2O of the *hcnA* 20-mer in complex with RsmE at 40°C. Prominent intermolecular NOEs to G14 and G11 are assigned. **(d)** Imino region of a 2D NOESY spectrum in H_2O of the *hcnA* 12-mer in complex with RsmE at 30°C. Very similar intermolecular NOEs to G14 and G11 as in the *hcnA* 20-mer complex are observed.

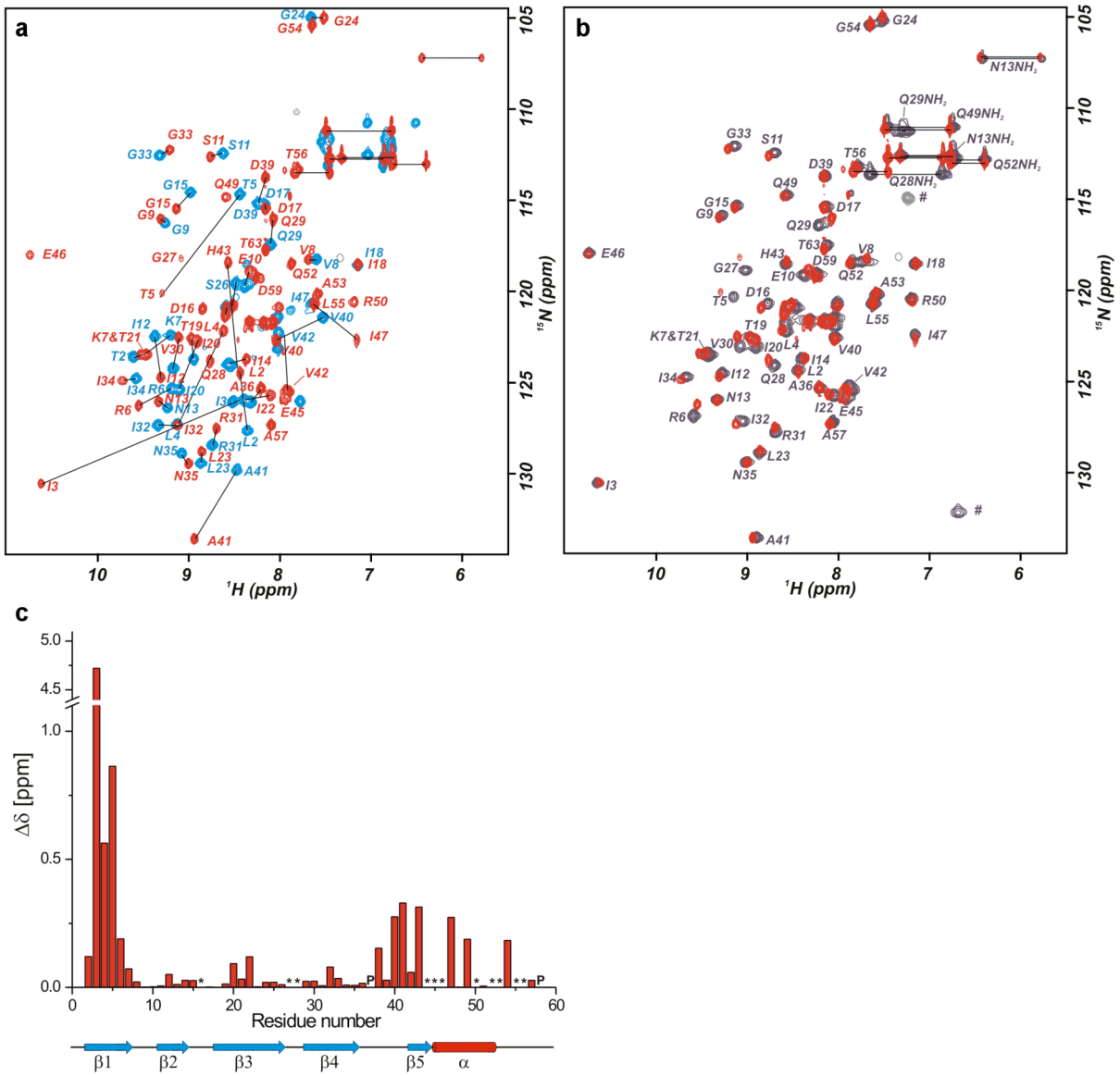

Figure S2: Chemical shift differences upon complexation of RsmE. (a) Overlay of ^{15}N-HSQC spectra of free RsmE (cyan) and RsmE bound to one equivalent of the *hcnA* 12-mer stem loop (red). **(b)** Overlay of ^{15}N-HSQC spectra of RsmE bound to one equivalent of the *hcnA* 12-mer (red) and RsmE bound to one equivalent of the *hcnA* 20-mer (dark grey). The # denotes folded side chain resonances. **(c)** Plot of the chemical shift difference between amide groups of the free and bound form of RsmE- *hcnA* 20-mer ($\delta = [\delta_{HN}^2 + (\delta_N/R_{scale})^2]^{1/2}$, $R_{scale} = \gamma_H/\gamma_N = 9.85$). An asterisk denotes residues not assigned in free RsmE due to the absence or very low intensity of signals. A **P** denotes prolines.

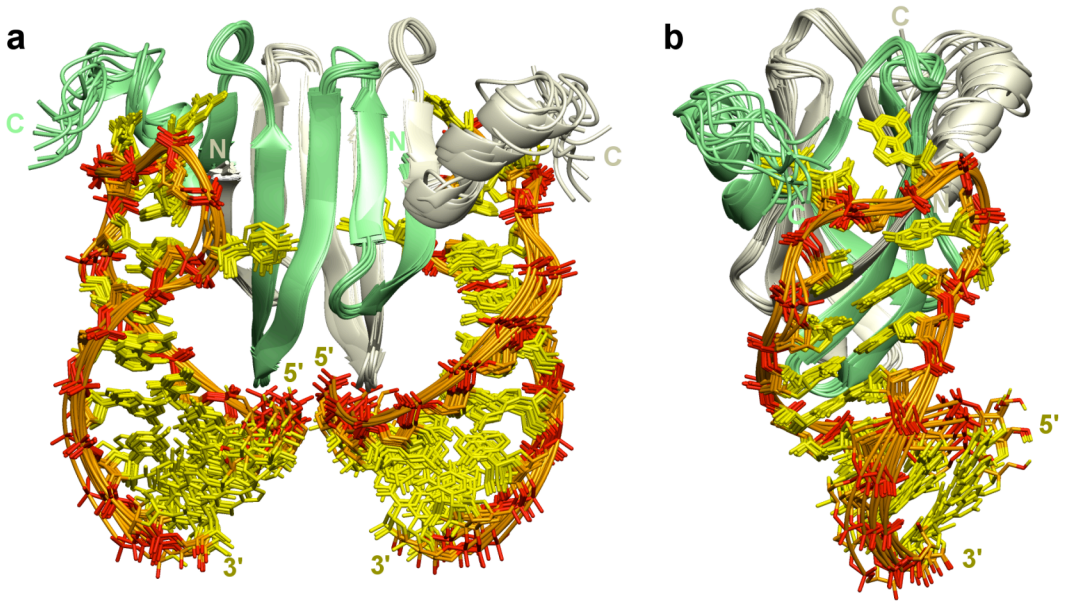

Figure S3: Structure ensemble of the RsmE-RNA complex. (a) 10 complex structures with the lowest energy in regard to violations of the distance constraints are superimposed. **(b)** Side view showing the ensemble for one RNA binding site.

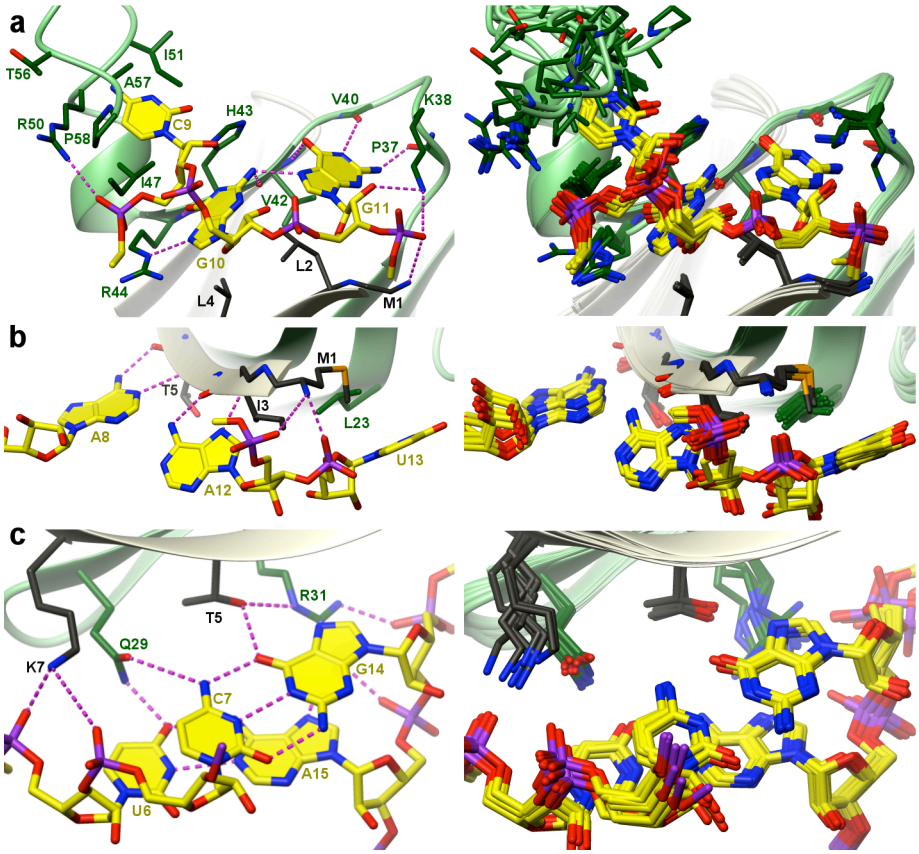

Figure S4: Precision of the NMR structure at the RNA-protein interface. Shown is a typical structure on the left and the whole ensemble of 10 structures with the lowest energy in regard to violations of the distance constraints in the right. **(a)** Recognition site of the nucleotides C_9, G_{10} and G_{11}. **(b)** Recognition of the nucleotides A_8 and A_{12}. **(c)** Recognition in the major groove of C_7-G_{14} and U_6-A_{15} base-pairs.

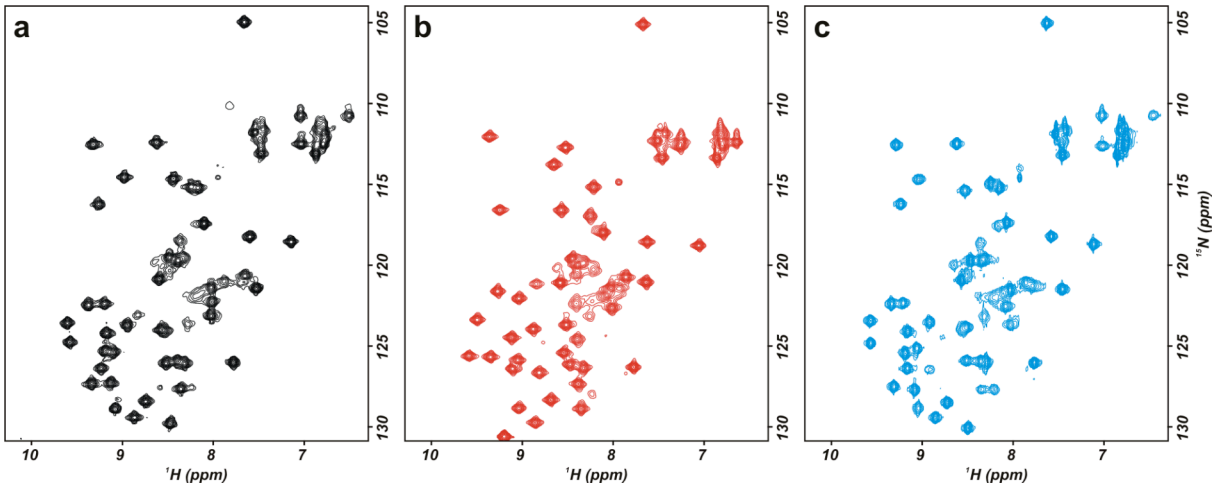

Figure S5: The L4A and R44A mutations do not impair the overall fold of RsmE. ^{15}N-HSQC spectra of free **(a)** Wild type (WT) RsmE in black, **(b)** L4A RsmE in red and **(c)** R44A RsmE in cyan.

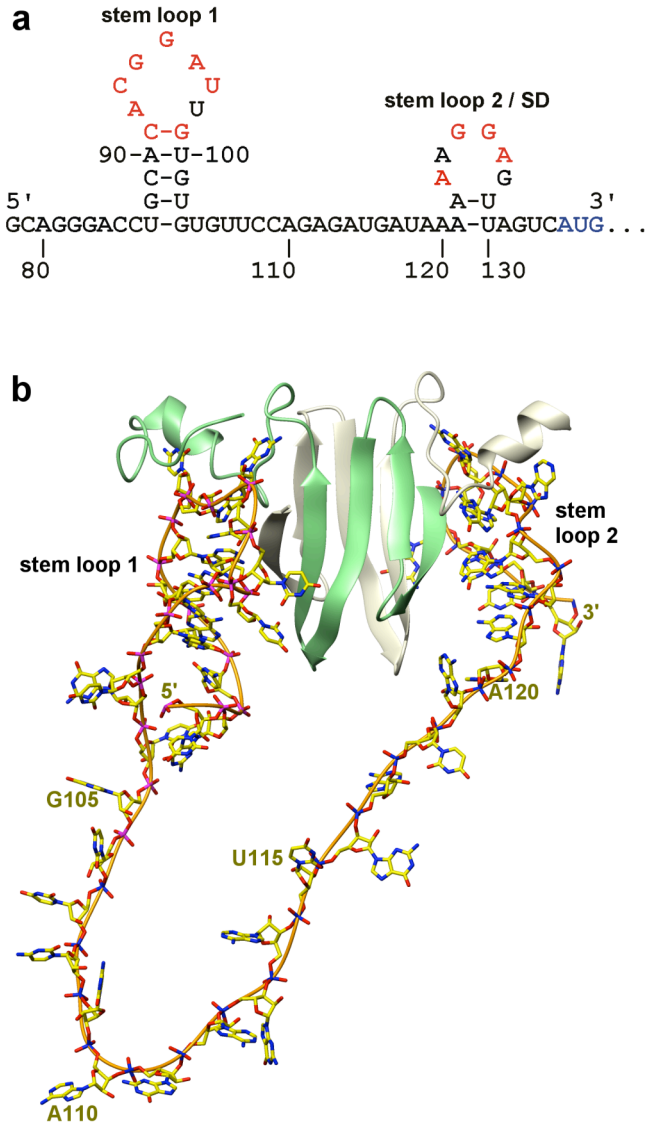

Figure S6: *Escherichia coli glgC* 5´ leader mRNA. (A) Schematic presentation of the assumed secondary structure of the *glgC* 5´ leader mRNA based on the homology to the RsmE-*hcnA* complex structure. Residues that are identical to motifs in the *hcnA* 5´ UTR are marked in red. AUG (blue) denotes the start codon. (B) Model of the *glgC* 5´ leader mRNA bound to RsmE.

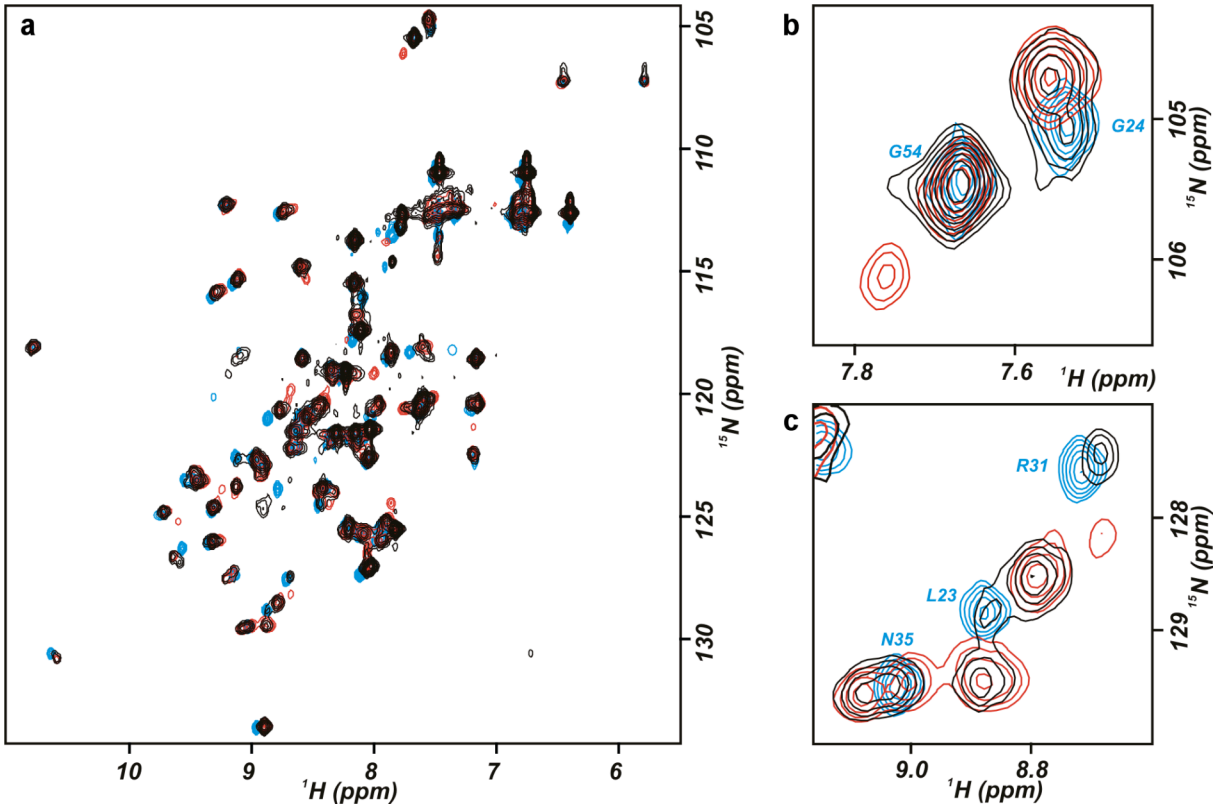

Figure S7: Two sets of chemical shifts are observed when RsmE is bound to one equivalent of the *hcnA* 50-mer (residues 58-104 plus GAG at 5´ end) indicating that two different GGA motifs of the same RNA are binding to one RsmE dimer. (a) Overlay of ^{15}N-HSQC spectra of the complex of RsmE bound to one equivalent of the *hcnA* 12-mer stem-loop containing the S-D sequence (cyan); RsmE bound to one equivalent of the *hcnA* 26-mer stem loop containing two GGA motifs downstream of the S-D (red) and RsmE bound to one equivalent of the *hcnA* 50-mer stem loop containing the S-D and the two upstream GGA motifs (black) at 40°C. **(b)** Close up of the overlay for residues G54 and G24. The two G24 signals of RsmE in complex with the 50-mer (black) resemble the G24 signal from the 12-mer complex plus the G24 signal from the 26-mer complex. In the structure G24 is in proximity of U13, the looped out base after the GGA motif of the S-D sequence. The sequences of the two additional GGA motifs within the 26- and 50-mer are different leading to different chemical shifts of G24 in complex. **(b)** Close up of the overlay for residues L23, R31 and N35. In the complex structure these residues are also located in the proximity of U13. The spectrum of RsmE in complex with the 50-mer (black) approximately resembles the signals from the 12-mer complex plus the signals from the 26-mer complex. The signals of the 26-mer complex contain two sets of signals of which only one is also found in the 50-mer complex.

Table S1. Bacterial strains, plasmids, and oligonucleotides used in this study

Strain, plasmid, or oligonucleotide	Relevant characteristics or sequence	Source or reference
E.coli		
BL21(DE3)	F^- *ompT hsdS*$_B$(r_B^- m_B^-) *gal dcm* (λDE3)	Novagen
BL21(DE3) Codon+ RIL	Strategene, *E. coli* B F^- *ompT hsdS* (r_B^- m_B^-) *dcm*$^+$ Tet^r *gal* (λDE3) *endA* Hte (*argU ileY leuW* Cam^r)	
P. fluorescens		
CHA0	WT	1
CHA89	*gacA*::Km^r	2
CHA1027	*rsmA*::│Km *rsmE*::│Hg *hcnA'-'lacZ*, Km^r Hg^r	3
pET28b	Expression vector, P_{T7}, Km^r	Novagen
pME6001	Cloning vector, pBBR1MCS derivative, Gm^r	4
pME6032	*lacI*^{Q}-P_{tac} expression vector	5
pME6533	pME3219 with artificial restriction sites KpnI and SphI in *hcnA* leader sequence; template for *in vitro* transcription of *hcnA* leader	4
pME6624	pME6533 derivative with oligonucleotides 6624 and 6624rev between KpnI and SphI sites	This study
pME6629	pME6533 derivative with oligonucleotides 6629 and 6629rev between KpnI and SphI sites	This study
pME6638	pME6533 derivative with oligonucleotides 6638 and 6638rev between KpnI and SphI sites	This study
pME6919	Template for *in vitro* transcription of *rsmY* under P_{T7}	6
pME6920	Template for *in vitro* transcription of *rsmZ* under P_{T7}	7
pME6926	Template for *in vitro* transcription of *carA* leader under P_{T7}	6
pME7013	pET28a derivative carrying *rsmE*, Km^r	3
pME7318	Template for *in vitro* transcription of *rsmX* under P_{T7}	8
pME7609	pET28b derivative carrying *rsmE*, Km^r	This study
pME7618	pME6032 derivative carrying *rsmE*-His_6, Km^r	This study
pME7633	pME6533 derivative with oligonucleotide fragments 7633 and 7633rev between KpnI and SphI sites	This study
pME9502	pME7618 mutant obtained by directed mutagenesis using oligonucleotides 9502 and 9502rev, RsmE L4A	This study
pME9503	pME7618 mutant obtained by directed mutagenesis using oligonucleotides 9503 and 9503rev, RsmE R6A	This study
pME9504	pME7618 mutant obtained by directed mutagenesis using oligonucleotides 9504 and 9504rev, RsmE R44A	This study
Oligonucleotides (5'→3')		
hcn	TGTAATACGACTCACTATAGGGGCTCGGTTCTGACAAACAGCTTGGG	This study
hcnrev	CGGAATTCTGCAGCGGCTGAATATCGAAG	This study
hcn15	TGTAATACGACTCACTATAGGGTTCACGGATGAA	This study
hcn15rev	TTCATCCGTGAACCCTATAGTGAGTCGTATTACA	This study
hcn20	TGTAATACGACTCACTATAGGGGGGCTTCACGGATGAAGCCC	This study
hcn20rev	GGGCTTCATCCGTGAAGCCCCCCTATAGTGAGTCGTATTACA	This study
PTZ	TCTAATACGACTCACTATAGGG	This study
PTZeco	ATGCGAATTCAAAAAAAACCCGCCGAAGCG	8
PTZrev	GGATCCTCTAGAGTCGACCTGC	This study
6624	CCCATTCATTTTTAACGGATGAACCCAGCATG	This study
6624rev	CTGGGTTCATCCGTTAAAAATGAATGGGGTAC	This study
6629	CCCATTCATTTTTCTCGGATGAACCCAGCATG	This study
6629rev	CTGGGTTCATCCGAGAAAAATGAATGGGGTAC	This study
6638	CCCATTCATTTTTCACGGCTGAACCCAGCATG	This study
6638rev	CTGGGTTCAGCCGTGAAAAATGAATGGGGTAC	This study
7633	CCCATTCATTTTTCACACATGAACCCAGCATG	This study
7633rev	CTGGGTTCATGTGTGAAAAATGAATGGGGTAC	This study
9502	GATATACCATGCTGATAGCCACCCGCAAAGTCGGTG	This study
9502rev	CACCGACTTTGCGGGTGGCTATCAGCATGGTATATC	This study
9503	CCATGCTGATACTCACCGCCAAAGTCGGTGAAAGC	This study
9503rev	GCTTTCACCGACTTTGGCGGTGAGTATCAGCATGG	This study
9504	GACGTCGCGGTACACGCGGAAGAAATCTATCAAC	This study
9504rev	GTTGATAGATTTCTTCCGCGTGTACCGCGACGTC	This study

Table S2: Intermolecular protein–RNA hydrogen bond constraints. Note that these constraints were only used in the final calculations. The orientations and positions of the bases are already defined without these hydrogen bond constraints.

Hydrogen bond constraints (per one protein–RNA subunit)	supporting chemical shift and hydrogen exchange data
$I3_A$ N - $A12_C$ N7	I3 H^N is protected from hydrogen exchange, large chemical shift change, see Fig. S2
$I3_A$ O – $A12_C$ N6	δ (C´)$_{free}$ = 175.6 ppm; δ (C´)$_{bound}$ = 174.3 ppm
$T5_A$ N - $A8_C$ N1	T5 H^N is protected from hydrogen exchange, large chemical shift change, see Fig. S2
$T5_A$ O - $A8_C$ N6	δ (C´)$_{free}$ = 175.7 ppm; δ (C´)$_{bound}$ = 177.2 ppm
$V42_B$ N – $G11_C$ O6	V42 H^N is protected from hydrogen exchange, large chemical shift change, see Fig. S2
$V42_B$ O – $G10_C$ N2	δ (C´)$_{free}$ = 175.4 ppm; δ (C´)$_{bound}$ = 173.0 ppm

Supplementary Methods

Bacterial strains and growth conditions. The bacterial strains, plasmids and oligonucleotides used in this study are listed in **Table S1**. *P. fluorescens* strains were routinely grown in nutrient yeast broth (NYB; 2.5% (w/v) nutrient broth, 0.5% (w/v) yeast extract) with shaking (180 rpm) at 30°C. Triton X-100 at 0.05% (w/v) was added to the liquid cultures to avoid cell aggregation. Antibiotics when required were added to the final concentrations: kanamycin, 50 mg ml^{-1}, for *E. coli* and *P. fluorescens*; tetracycline, 125 g ml^{-1}, and gentamicin, 10 g ml^{-1}, for *P. fluorescens*.

DNA manipulations. They were carried out with standard protocols (Sambrook and Russel 2001). Plasmid inserts were generated by restriction digestion or PCR using Taq DNA polymerase (Eppendorf) and gene-specific primers containing restriction sites. Mutagenesis was carried out using the QuikChange site-directed mutagenesis kit (Stratagene). Chromosomal DNA was prepared as previously described[9]. Mutations were confirmed by nucleotide sequencing (Microsynth).

RsmE-*hcnA* RNA complex formation (12-mer and 20-mer). The His-tagged RsmE (RsmE6H) protein was overexpressed in *E. coli* BL21(DE3)+RIL/pME7013 at 37°C in minimal medium M9 containing 1 g l^{-1} $^{15}NH_4Cl$ and 4 g l^{-1} glucose (for ^{15}N-labeled proteins) or 1 g l^{-1} $^{15}NH_4Cl$ and 2 g l^{-1} ^{13}C-glucose (for $^{13}C/^{15}N$ labeled proteins) and 50 mg l^{-1} kanamycin. Cell cultures were induced at OD_{600}~0.6 by 1 mM isopropyl β-D-thiogalactoside at 37°C. Cells were harvested after 4 h by centrifugation. For purification, Ni-NTA metal-affinity chromatography was used following the manufacturer's instructions (Qiagen Inc.) except that an additional washing step with a high salt buffer (1 M NaCl, 50 mM Na_2HPO_4, pH 8.0, 10 mM imidazole) was added. After elution, the protein was dialyzed against NMR buffer (300 mM NaCl, 50 mM K_2HPO_4 pH 8.0) and concentrated to ~0.5 mM by centrifugation at 4°C using a 3 kDa molecular mass cut-off membrane (Vivascience). Identity and purity were verified by SDS-Tricine-PAGE and the absence of RNases was confirmed by the RNase Alert Lab Kit (Ambion).

For binding studies unlabeled *hncA* 12-mer (5´-UUCACGGAUGAA-3´) was purchased from Dharmacon Research, deprotected according to the instructions of the manufacturer, desalted using a G-15 size exclusion column (Amersham), adjusted to pH 7.2, lyophilized and dissolved in water. For structure determination, *hncA* 20-mer (5´-GGGCUUCACGGAUGAAGCCC-3´) was used with three different labeling schemes. Unlabeled RNA samples and two $^{13}C/^{15}N$-labeled RNA samples (with only G and U or with only C and A labeled) were produced by *in*

vitro run-off transcription with T7 polymerase and purified by anion-exchange high-pressure liquid chromatography under denaturing conditions. The oligonucleotides were annealed at low salt and pH 7.2 by heating to 95°C and snap-cooling on liquid nitrogen to favor a stem-loop conformation.

The complexes were prepared by titrating the concentrated RNA solution of typically 10 mM into a ~0.5 mM solution of RsmE in 300 mM NaCl, 50 mM K_2HPO_4 (pH 8.0) buffer until a 1:1 stoichiometry was reached. Subsequently, the buffer was exchanged to 30 mM NaCl and 50 mM K_2HPO_4 (pH 7.2) with a Centricon (5 kDa molecular mass cut-off membrane, Vivascience) device. Concentrations were determined by UV spectroscopy ($\varepsilon_{Protein,280}$ = 1490 M^{-1} cm^{-1}; $\varepsilon_{RNA,260}$ (20-mer) = 191,300 M^{-1} cm^{-1}; $\varepsilon_{RNA,260}$ (12-mer) = 125,100 M^{-1} cm^{-1}) and Bradford protein assay (Bio-Rad).

Preparation of RsmE mutants. The His-tagged RsmE containing either a L4A or R44A mutation was overexpressed in *E. coli* BL21(DE3)+RIL (plasmids pME9502 and pME9504, respectively) at 37°C in minimal medium M9 containing 1 g l^{-1} $^{15}NH_4Cl$ and 4 g l^{-1} glucose and 50 mg l^{-1} kanamycin. The proteins were purified in the same way as the wild type protein.

RsmE-*hcnA* RNA complex formation (26-mer and 50-mer). Unlabeled *hncA* 26-mer (5´-GAGCAUGGACGGCGGGACGCCGGGUA-3´) and 50-mer (5´-GAGCAUGGACGGCGGGACGCCGGGUACCCCAUUCAUUUUUCACGGAUGAA-3´) were produced by *in vitro* run-off transcription with T7 polymerase and purified by anion-exchange high-pressure liquid chromatography under denaturing conditions. The complexes were prepared by mixing the concentrated RNA solution of typically 2 mM with a ~0.5 mM solution of RsmE in 300 mM NaCl, 50 mM K_2HPO_4 (pH 8.0) buffer in a 1:1 stoichiometry. Subsequently, the buffer was exchanged to 30 mM NaCl and 50 mM K_2HPO_4 (pH 7.2) with a Centricon (5 kDa molecular mass cut-off membrane, Vivascience) device. Concentrations of the RNA were determined by UV spectroscopy ($\varepsilon_{RNA,260}$ (26-mer) = 258,000 M^{-1} cm^{-1}; $\varepsilon_{RNA,260}$ (50-mer) = 490,700 M^{-1} cm^{-1}).

NMR spectroscopy. NMR spectra were acquired on DRX-500, DRX-600 and Avance 900 Bruker spectrometers equipped with inverse triple resonance probes and pulse field gradient accessory. Unless indicated otherwise data were measured at 40°C. NMR data were processed using XWINNMR and NMRPipe[10] and analyzed with Sparky[11]. The ^1H,^{13}C,^{15}N chemical shifts of the protein, free and in complex, were assigned by standard methods[12].

RNA resonance assignments of the complex was achieved using 2D ^1H-^1H TOCSY, 2D ^1H-^1H NOESY and 2D ^1H-^1H double-half-filtered NOESY[13] spectra collected on a ^{13}C,^{15}N-labeled

protein, in complex with unlabeled RNA, in 100% ^2H_2O. Additionally, 3D ^{13}C-edited NOESY and 3D HCCH-TOCSY experiments collected on complexes of ^{15}N-labeled RsmE in complex with either $^{13}C/^{15}N$-GU labeled or $^{13}C/^{15}N$-CA labeled *hncA* 20-mer in 100% ^2H_2O was used in order to unambiguously assign the sugar resonances.

The assignments of intermolecular NOEs were based on 3D ^{13}C F_1-edited, F_3-filtered NOESY-HSQC[14] and a 2D ^1H-^1H F_1-^{13}C-filtered F_2-^{13}C-edited NOESY[13] spectra of the protein-RNA complex with either the protein $^{13}C/^{15}N$ labeled and the RNA unlabeled or the protein ^{15}N-labeled and the RNA $^{13}C/^{15}N$ labeled.

Amide ^{15}N T_1, T_2 and steady-state heteronuclear $^1H\{^{15}N\}$NOE relaxation experiments[15] for ^{15}N labeled RsmE-*hncA* 20-mer were recorded on a DRX-600 Bruker spectrometer. The correlation time τ_C was estimated from an average T_1/T_2 ratio of the rigid amides according to Gryk et al[16].

Structure calculation and refinement. Preliminary structures of the RsmE-RNA complex were obtained by a simulated annealing protocol using the DYANA package[17] and manually assigned NOE distance constraints. 100 structures were generated by DYANA starting from random RNA and protein starting structures and 30,000 simulated annealing steps. Initial calculations with an RsmE monomer and one RNA did not converge. Over 100 NOE distance restraints can only be satisfied by a RsmE dimer with a CsrA fold and were thus classified as intermolecular restraints. This is supported by amide signals protected from hydrogen exchange at the dimerization interface (between strands $\beta1_A$ and $\beta4_B$; $\beta2_A$ and $\beta5_B$ and vice versa). At later stages of the refinement, hydrogen-bond restraints including six intermolecular one (three from slowly exchanging amides and three from significant chemical shift perturbations in the carbonyl, see Table S2) were added. To impose better convergence of the ensemble, Watson-Crick hydrogen-bonds and some artificial torsion angle restraints for the A-form RNA double-helical range were used. This set of torsion angles was derived from the high-resolution crystal structures as described earlier[18]. An ensemble of 20 structures, selected based on the lowest target function, served for the refinement in AMBER 7.0[19].

The complex was refined in implicit solvent using NOE-derived distances, torsion angles and hydrogen bond restraints as summarized in Table 1. In all AMBER calculations, the force-field 98 based on the Cornell et al[20]. force-field was used along with the generalized Born model[21] to mimic solvent. A 20-ps simulated annealing protocol consisting of 20,000 steps was used. Square-well penalty functions were used for all NMR restraints with the force constants 50 kcal mol^{-1} $Å^{-2}$ and 200 kcal mol^{-1} rad^{-2} for distance constraints and torsion angles, respectively. The relative weights of the valence-angle energy, torsion energy and 'improper' torsional terms were gradually increased during the simulated annealing to maintain the planarity of aromatic rings and proper local geometries. The simulated annealing protocol was followed by a short energy

minimization of 400 cycles (a combination of steepest-descents minimization followed by conjugate gradient technique). Ten conformers with the lowest distance violations were selected to obtain the final ensemble of structures. The quality of the complex was analyzed by PROCHECK[22] and NUCHECK[23].
Figures of the complex structure were prepared using MOLMOL[24] and PYMOL[25].

Modelling of a RsmE-*glgC* complex. Model structures of the RsmE-*glgC* complex (Fig. S6) were obtained by a simulated annealing protocol using the DYANA package identical to the one described above. For stem-loop residues identical to the *hncA* 20-mer, distance restraints from the RsmE-*hncA* complex were used. Additionally, Watson-Crick hydrogen-bonds and artificial torsion angle restraints for the A-form RNA double-helical range were used.

Supplementary references:

1. Voisard, C. et al. Biocontrol of root diseases by Pseudomonas fluorescens CHA0: current concepts and experimental approaches, p. 67-89. *In F. O'Gara, D. Dowling, and B. Boesten (ed.), Molecular ecology of rhizosphere microorganisms. VCH Publishers, Weinheim, Germany* (1994).
2. Laville, J. et al. Global Control in Pseudomonas-Fluorescens Mediating Antibiotic-Synthesis and Suppression of Black Root-Rot of Tobacco. *Proceedings of the National Academy of Sciences of the United States of America* **89**, 1562-1566 (1992).
3. Reimmann, C., Valverde, C., Kay, E. & Haas, D. Posttranscriptional repression of GacS/GacA-controlled genes by the RNA-binding protein RsmE acting together with RsmA in Biocontrol strain Pseudomonas fluorescens CHA0. *Journal of Bacteriology* **187**, 276-285 (2005).
4. Blumer, C., Heeb, S., Pessi, G. & Haas, D. Global GacA-steered control of cyanide and exoprotease production in Pseudomonas fluorescens involves specific ribosome binding sites. *Proc Natl Acad Sci U S A* **96**, 14073-8 (1999).
5. Heeb, S., Blumer, C. & Haas, D. Regulatory RNA as mediator in GacA/RsmA-dependent global control of exoproduct formation in Pseudomonas fluorescens CHA0. *J Bacteriol* **184**, 1046-56 (2002).
6. Valverde, C., Heeb, S., Keel, C. & Haas, D. RsmY, a small regulatory RNA, is required in concert with RsmZ for GacA-dependent expression of biocontrol traits in Pseudomonas fluorescens CHA0. *Mol Microbiol* **50**, 1361-79 (2003).
7. Valverde, C., Lindell, M., Wagner, E.G.H. & Haas, D. A repeated GGA motif is critical for the activity and stability of the riboregulator RsmY of Pseudomonas fluorescens. *Journal of Biological Chemistry* **279**, 25066-25074 (2004).
8. Kay, E., Dubuis, C. & Haas, D. Three small RNAs jointly ensure secondary metabolism and biocontrol in Pseudomonas fluorescens CHA0. *Proceedings of the National Academy of Sciences of the United States of America* **102**, 17136-17141 (2005).
9. Gamper, M., Ganter, B., Polito, M.R. & Haas, D. Rna Processing Modulates the Expression of the Arcdabc Operon in Pseudomonas-Aeruginosa. *Journal of Molecular Biology* **226**, 943-957 (1992).
10. Delaglio, F. et al. Nmrpipe - a Multidimensional Spectral Processing System Based on Unix Pipes. *Journal of Biomolecular Nmr* **6**, 277-293 (1995).
11. Goddard, T.D. & Kneller, D.G. *Sparky 3, Univ. of California, San Francisco*.
12. Sattler, M., Schleucher, J. & Griesinger, C. Heteronuclear multidimensional NMR experiments for the structure determination of proteins in solution employing pulsed field gradients. *Progress in Nuclear Magnetic Resonance Spectroscopy* **34**, 93-158 (1999).
13. Peterson, R.D., Theimer, C.A., Wu, H.H. & Feigon, J. New applications of 2D filtered/edited NOESY for assignment and structure elucidation of RNA and RNA-protein complexes. *Journal of Biomolecular Nmr* **28**, 59-67 (2004).
14. Lee, W., Revington, M.J., Arrowsmith, C. & Kay, L.E. A pulsed field gradient isotope-filtered 3D 13C HMQC-NOESY experiment for extracting intermolecular NOE contacts in molecular complexes. *FEBS Lett* **350**, 87-90 (1994).
15. Farrow, N.A. et al. Backbone Dynamics of a Free and a Phosphopeptide-Complexed Src Homology-2 Domain Studied by N-15 Nmr Relaxation. *Biochemistry* **33**, 5984-6003 (1994).
16. Gryk, M.R., Abseher, R., Simon, B., Nilges, M. & Oschkinat, H. Heteronuclear relaxation study of the PH domain of beta-spectrin: Restriction of loop motions upon binding inositol trisphosphate. *Journal of Molecular Biology* **280**, 879-896 (1998).
17. Guntert, P., Mumenthaler, C. & Wuthrich, K. Torsion angle dynamics for NMR structure calculation with the new program DYANA. *Journal of Molecular Biology* **273**, 283-298 (1997).

18. Oberstrass, F.C. et al. Shape-specific recognition in the structure of the Vts1p SAM domain with RNA. *Nature Structural & Molecular Biology* **13**, 160-167 (2006).
19. Case, D.A. et al. *AMBER Version 7 (Univ. of California, San Francisco, USA)* (2002).
20. Cornell, W.D. et al. A 2nd Generation Force-Field for the Simulation of Proteins, Nucleic-Acids, and Organic-Molecules. *Journal of the American Chemical Society* **117**, 5179-5197 (1995).
21. Bashford, D. & Case, D.A. Generalized born models of macromolecular solvation effects. *Annual Review of Physical Chemistry* **51**, 129-152 (2000).
22. Laskowski, R.A., Rullmann, J.A.C., MacArthur, M.W., Kaptein, R. & Thornton, J.M. AQUA and PROCHECK-NMR: Programs for checking the quality of protein structures solved by NMR. *Journal of Biomolecular Nmr* **8**, 477-486 (1996).
23. Feng, Z., Westbrook, J. & Berman, H.M. *Report NDB -470 (Rutgers Univ., New Brunswick, N.J.)* (1998).
24. Koradi, R., Billeter, M. & Wuthrich, K. MOLMOL: A program for display and analysis of macromolecular structures. *Journal of Molecular Graphics* **14**, 51-& (1996).
25. DeLano, W.L. The PyMOL Molecular Graphics System (DeLano Scientific, San Carlos, CA, USA). (2002).